

Article

Struvite Grown in Gel, Its Crystal Structure at 90 K and Thermoanalytical Study

Jolanta Prywer ^{1,*} , Lesław Sieroń ²  and Agnieszka Czyłkowska ² ¹ Institute of Physics, Lodz University of Technology, Wólczańska 219, 90-924 Łódź, Poland² Institute of General and Ecological Chemistry, Lodz University of Technology, Zeromskiego 116, 90-924 Łódź, Poland; leslaw.sieron@p.lodz.pl (L.S.); agnieszka.czyłkowska@p.lodz.pl (A.C.)

* Correspondence: jolanta.prywer@p.lodz.pl; Tel.: +48-42-631-3653

Received: 21 December 2018; Accepted: 31 January 2019; Published: 8 February 2019



Abstract: In this article, we report the crystallization of struvite in sodium metasilicate gel by single diffusion gel growth technique. The obtained crystals have a very rich morphology displaying 18 faces. In this study, the habit and morphology of the obtained struvite crystals are analyzed. The crystals were examined and identified as pure struvite by single X-ray diffraction (XRD). The orthorhombic polar noncentrosymmetric space group $Pmn2_1$ was identified. The structure of the crystal was determined at a temperature of 90 K. Our research indicates a lack of polymorphism, resulting from the temperature lowering to 90 K, which has not been previously reported. The determined unit cell parameters are as follows $a = 6.9650(2) \text{ \AA}$, $b = 6.1165(2) \text{ \AA}$, $c = 11.2056(3) \text{ \AA}$. The structure of struvite is presented here with a residual factor $R1 = 1.2\%$ at 0.80 \AA resolution. We also present thermoanalytical study of struvite using thermal analysis techniques such as thermogravimetry (TG), derivative thermogravimetry (DTG) and differential thermal analysis (DTA).

Keywords: crystal growth; crystallization; morphology; crystal structure; phosphates; thermal decomposition; magnesium compounds; struvite structure; struvite; growth from gel; magnesium ammonium phosphates hexahydrate

1. Introduction

Practical attempts to obtain crystals in the gel environment were made in the 1960s [1]. A gel is a two-component system with mechanical properties of a solid body, however, containing a large number of microscopic liquid phase. This structure provides adequate stiffness, eliminating convection, while maintaining the mobility of ions close to that observed during crystal growth from solutions. Initially, gel techniques have been found to be particularly useful for obtaining crystals of compounds that are sparingly soluble in water and metal crystals, due to the difficulty of obtaining these crystals from solutions and melts. With regard to these substances, the gel method proved to be very effective, because it allows obtaining single crystals at room temperatures, without the use of complicated and expensive equipment. The progress in technology has led to such development of gel techniques that nowadays one can obtain crystals of many inorganic and organic substances, including substances well soluble in water and metals. Currently, increased interest in organic crystals makes the gel crystallization processes become important not only from the point of view of crystal growth technology development but also of intensive interdisciplinary research in physics, chemistry, medicine and pharmacology. The development of gel techniques proceeds in two main directions. The first is the use of gel methods for obtaining crystals, including those of complex organic compounds, for example, proteins, nucleic acids and viruses [2–5]. Potentially very interesting is the use of gel methods for the production of drugs [6,7]. Another important reason for the increasing interest in gel methods is that the course of many processes occurring in the gel is very similar to the course of processes

occurring in living tissues. This allows the study of phenomena related, for example, to the formation of bone tissues, the formation of urinary and biliary stones [8], the influence of drugs on processes of pathological crystallization or the course of enzymatic processes [9].

As the crystal growth in a gel medium is a powerful method for growing high-quality crystals, we decided to grow magnesium ammonium phosphate hexahydrate ($\text{MgNH}_4\text{PO}_4 \cdot 6\text{H}_2\text{O}$) crystal, known as struvite, from sodium metasilicate gel and to study its structure and thermal decomposition.

Struvite is a mineral first identified and described as occurring in sewers, specifically in the St. Nikolai church in Hamburg, Germany [10]. This mineral was named a struvite for honouring Heinrich Christoph Gottfried Struve (1772–1851), the Russian Consul of Hamburg, who held this function at a time when this mineral was discovered. [11]. We now know that struvite is a fascinating inorganic material and its crystallization has been widely investigated over the last decade for several reasons.

Firstly, struvite can be a problem in sewage and wastewater treatment as it precipitates easily on specific locations, which may clog the system pipes [12–18]. The formation of struvite is strongly correlated with wastewater pH level. An increasing pH level of the wastewater increases the potential of struvite crystallization. The most common locations for initial struvite formation and subsequent build-up are points with high turbulence such as elbows of pipe connections, valves, aeration assemblies and pump internal components exposed to wastewater. At these zones of turbulence, carbon dioxide is released. This is known as degassing process which leads locally to an increase in pH. The sites with locally higher pH level are advisable for struvite formation. Struvite also has a greater tendency to form on rough surfaces. In favourable conditions, struvite may grow rapidly leading to clog system pipes.

On the other hand, struvite is a potential source of phosphorus, nitrogen and magnesium and therefore it is a main compound recovered from wastewater and converted into useful fertilizer containing these elements (for example Refs. [19–23]). The recovery of struvite from wastewater is especially essential in view of phosphorus [15,24,25]. Nowadays natural sources of heavy metal-free phosphorus are becoming scarce. At the same time, phosphorus content in sewage sludge is a growing environmental concern. That is why the recovery of phosphorus from wastewater is very essential. In addition to nitrogen and potassium, phosphorus is one of three main elements necessary for plants life. Deficiency of phosphorus causes different undesirable symptoms in plants, for example the slowdown of their growth. Therefore, many fertilizers contain phosphates and the recovery of phosphorus from sewage, in particular from struvite, is very essential.

The third and the most important reason for which struvite has been studied for last years is the fact that it is the main component of the so-called infectious urinary stones, related to urinary tract infection [26–30]. The infection is a result of the activity of microorganisms producing urease, mainly from *Proteus* species. Urease, a bacterial enzyme, catalyzes the hydrolysis of urea, to form ammonia. This decomposition of urea initiates a cascade of reactions leading to an increase in urine pH, which results in an elevation of the concentration of NH_4^+ , CO_3^{2-} and PO_4^{3-} ions. These ions together with the ions of magnesium Mg^{2+} present in urine lead to the crystallization of struvite [29]. Infectious urinary stones are a problem that has been widespread for ages, however, in the last quarter of the century, the incidence of infectious urolithiasis increased by 60–75%. Infectious urinary stones account for up to 30% of all urinary stones [31,32] and are a very serious health problem. Studies show that in highly developed countries there is a systematic increase in incidence of infectious urolithiasis, which indicates that infectious urinary stones are a social problem.

According to the literature review presented, struvite is an interesting inorganic material worth testing. As already mentioned, the goal of this work is to grow the struvite crystal by the gel method, to study its structure and thermal decomposition. The crystal structure of struvite has been previously reported by Whitaker and Jeffery [33], by Abbona, Calleri and Ivaldi [34] and by Tansman, Kindstedt and Hughes [35] from single crystal X-ray diffraction data as well as by Ferraris, Fuess and Joswig [36] from neutron diffraction data, all at room temperature.

In this article we present the structure of the struvite crystal examined at 90 K. XRD analysis at low temperatures gives the possibility to study phase transitions. So far, low-temperature X-ray diffraction analysis for struvite in the context of phase transitions has not been carried out.

The second goal of our research is to study the thermal decomposition of struvite. The thermal decomposition of struvite has also been studied in the past (e.g., Refs. [37–40]). Thermal decomposition made by us differs from that described in the literature. Therefore, it is advisable to include our thermolysis results in this paper.

2. Materials and Methods

2.1. Struvite Crystals Growth from Gel Medium

All used chemicals of reagent-grade purity were purchased from Sigma Aldrich. To prepare gel we used sodium metasilicate anhydrous (Na_2SiO_3 ; SMS), ammonium dihydrogenphosphate ($\text{NH}_4\text{H}_2\text{PO}_4$; ADP) and magnesium acetate tetrahydrate ($(\text{CH}_3\text{COO})_2\text{Mg}\cdot 4\text{H}_2\text{O}$). The chemicals were dissolved in distilled water. An aqueous solution of ADP of concentration of 0.38 M and SMS solution of specific gravity 1.07 were mixed together in appropriate amounts to adjust the pH of the mixture equal to 9.0. The prepared mixture was poured into tubes of 19 cm in length and 3 cm in diameter and left for gelation for 24 h. After the gelation, 25 mL of magnesium acetate tetrahydrate solution of 1 M was gently poured on the surface of newly-formed gel in respective tubes and closed with airtight cover. The crystal growth usually lasted from three to four weeks. After this time the crystals of struvite of about 1 mm in size along the *b*-axis were observed. Growth conditions were selected specifically to obtain crystals up to 1 mm in size, because crystals of this size are desirable for testing on a single-crystal diffractometer.

2.2. Instrumentation

The grown crystals were examined and identified as pure struvite by X-ray diffraction (XRD). Single crystal X-ray diffraction data were collected at 90 K by the ω -scan technique using a RIGAKU XtaLAB Synergy, Dualflex, Pilatus 300 K diffractometer [41] with PhotonJet micro-focus X-ray Source Mo-K α ($\lambda = 0.71073 \text{ \AA}$).

The thermal properties of struvite in air were studied by Thermogravimetry-Differential Thermal Analysis (TG-DTA) techniques in the range of temperature 25–1000 °C at a heating rate of 10 °C·min^{−1}; TG and DTA curves were recorded on TG 209 F1 Iris apparatus (Netzsch, Germany) under dry air atmosphere with flow rate $v = 20 \text{ mL}\cdot\text{min}^{-1}$, a ceramic crucible was used as reference material.

2.3. Data Collection, Structure Determination and Refinement

Data collection, cell refinement, data reduction, and absorption correction were carried out with the CrysAlis PRO [41]. The crystal structure was solved by using direct methods with the SHELXT 2018/2 program [42]. Atomic scattering factors were taken from the International Tables for X-ray Crystallography. Positional parameters of non-H-atoms were refined by the full-matrix least-squares method with anisotropic thermal parameters by using the SHELXL 2018/3 program [43]. All hydrogen atoms were located using difference Fourier techniques and refined freely with isotropic temperature factors. Relevant crystallographic data and details of the experimental conditions are summarized in Table 1.

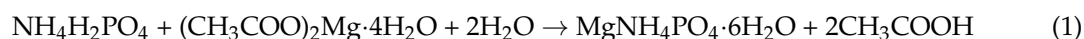
Table 1. Crystal data and structure refinement for struvite.

Formula	MgNH ₄ PO ₄ ·6H ₂ O
Formula weight	245.42
Crystal system	Orthorhombic
Space group	<i>Pmm</i> 2 ₁ (No. 31)
<i>a</i> (Å)	6.9650(2)
<i>b</i> (Å)	6.1165(2)
<i>c</i> (Å)	11.2056(3)
<i>V</i> (Å ³)	477.38(2)
<i>Z</i>	2
ρ (calculated) (g/cm ³)	1.707
F (000)	260
μ (mm ⁻¹)	0.389
Absorption correction	Analytical numeric
Temperature (K)	90
Wavelength (Å)	0.71073
θ (deg)	3.44–26.36
Index range	$-8 \leq h \leq 8, -7 \leq k \leq 7, -14 \leq l \leq 14$
R_{int}	0.019
Reflections collected	12286
Independent reflections	1061
Reflections ($I > 2\sigma(I)$)	1060
Completeness	99.8%
Data/Restraints/Parameters	1061/1/107
R1/wR2 ($I > 2\sigma(I)$)	0.0121/0.0333
R1/wR2 (all data)	0.0121/0.0333
GOF on F ²	1.14
Largest diff. peak and hole (e/Å ⁻³)	0.24 and -0.19
Weighting: $w = 1/[\sigma^2(F_o^2) + (0.0229P)^2 + 0.0413P]$ where $P = (F_o^2 + 2F_c^2)/3$	

3. Results and Discussion

3.1. Struvite Synthesis, Morphology and Habit

The single diffusion gel growth technique was used to grow struvite. Struvite is formed from two components, ADP (NH₄H₂PO₄) and magnesium acetate tetrahydrate (CH₃COO)₂Mg·4H₂O), according to the following reaction:



The grown struvite crystals show different morphologies, namely dendritic, and prismatic and rectangular platelet depending on the growth site. At the interface between the gel and the liquid phase, small dendritic type crystals were observed, while at greater depths in the gel (deeper below the gel-liquid interface) crystals in the form of rectangular platelets and prisms were observed. At the interface between gel and liquid there is a higher concentration of reagents, which results in the formation of dendrites. Regardless of morphology, struvite crystals are transparent. The size of both prismatic and rectangular crystals did not exceed 1 mm in the length of the *b*-axis. Growth conditions were intentionally selected so as to obtain the crystals of this size needed for XRD measurements. Figure 1 shows struvite crystals in gel medium.

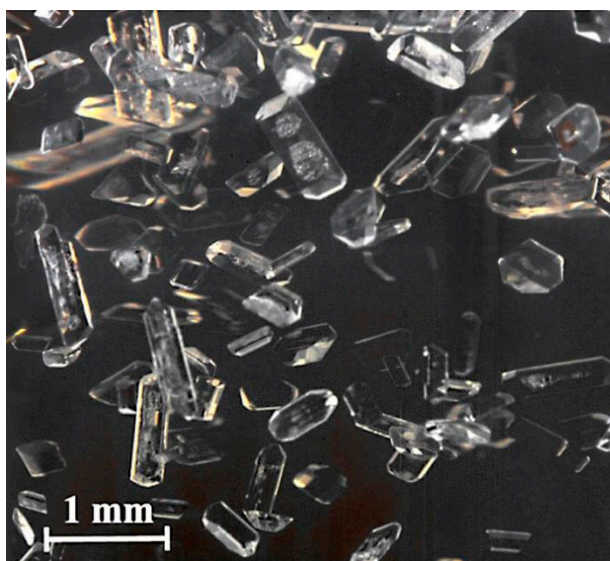


Figure 1. Struvite crystals in sodium metasilicate gel.

The most typical habit of struvite crystals obtained by us, using the single diffusion gel growth technique, is prismatic habit shown in Figure 2a,b and Movie S1 (in the Supplementary Material). The crystals are composed of the (001) and (00 $\bar{1}$) pedions, the {10 $\bar{1}$ }, {0 $\bar{1}$ 1}, {101} and {0 $\bar{1}\bar{1}$ } domes, the {110} rhombic prism and the {111} rhombic pyramid. Struvite exhibits hemimorphic morphology, which means that the faces at the two ends of the crystallographic *c*-axis are not related by symmetry elements. Therefore, the (001) and (00 $\bar{1}$) faces, which are at the ends of the *c*-axis, are single faces (pedions) not related to each other by symmetry. Domes are two non-parallel faces related with each other by a plane of symmetry (mirror plane). The {10 $\bar{1}$ } form is a dome consisting of the two (10 $\bar{1}$) and ($\bar{1}$ 0 $\bar{1}$) faces. The {0 $\bar{1}$ 1} form is also a dome consisting of the two (0 $\bar{1}$ 1) and (011) faces. Similarly the {101} form is a dome consisting of the two (101) and ($\bar{1}$ 01) faces, and the {0 $\bar{1}\bar{1}$ } dome is a two faced form consisting of the (0 $\bar{1}\bar{1}$) and (0 $\bar{1}\bar{1}$) faces. Rhombic prism is a four-faced form with all faces parallel to a common line. In the case of struvite the four faces (110), ($\bar{1}\bar{1}$ 0), ($\bar{1}\bar{1}$ 0) and ($\bar{1}$ 10) belong to the rhombic prism {110}. Rhombic pyramid is a four-faced form whose faces are related by mirror planes. In struvite the (111), ($\bar{1}\bar{1}$ 1), ($\bar{1}\bar{1}$ 1) and ($\bar{1}$ 11) faces are the four faces of the rhombic pyramid {111}. In total, struvite possess 18 faces.

The crystals that are terminated by pedions (001) and (00 $\bar{1}$) at both ends of the *c*-axis are quite common. Usually the (00 $\bar{1}$) pedion is larger than the (001) one. The habit of crystals with the smaller (001) pedion at the end of the *c*-axis is the so-called coffin-lid habit described widely in literature [44–46]. Sometimes it happens that the (001) face disappears completely and is not represented in the crystal morphology. If the (001) pedion disappears, the remaining (101) and ($\bar{1}$ 01) faces of the {101} form make an edge. The coffin-lid habit with or without the (001) face is typical for crystals growing in living animal [47] and human [44,46,48] organisms.

In the paper [34] the authors considered the correct assignment of struvite crystal face indexes (in particular (001) and (00 $\bar{1}$)) on the basis of the determined polarity. In this case, as in all other polar crystals, determination of the crystal face indexes depends on the initial assumption of the coordinate system. The unit-cell transformation using the matrix of

$$\begin{bmatrix} -1 & 0 & 0 \\ 0 & 1 & 0 \\ 0 & 0 & -1 \end{bmatrix} \quad (2)$$

gives an alternative set of crystal faces characterized by opposite indexes (Figure 2c). The correct polarity for the assumed coordinate system can be then confirmed, for example, using the Flack parameter.

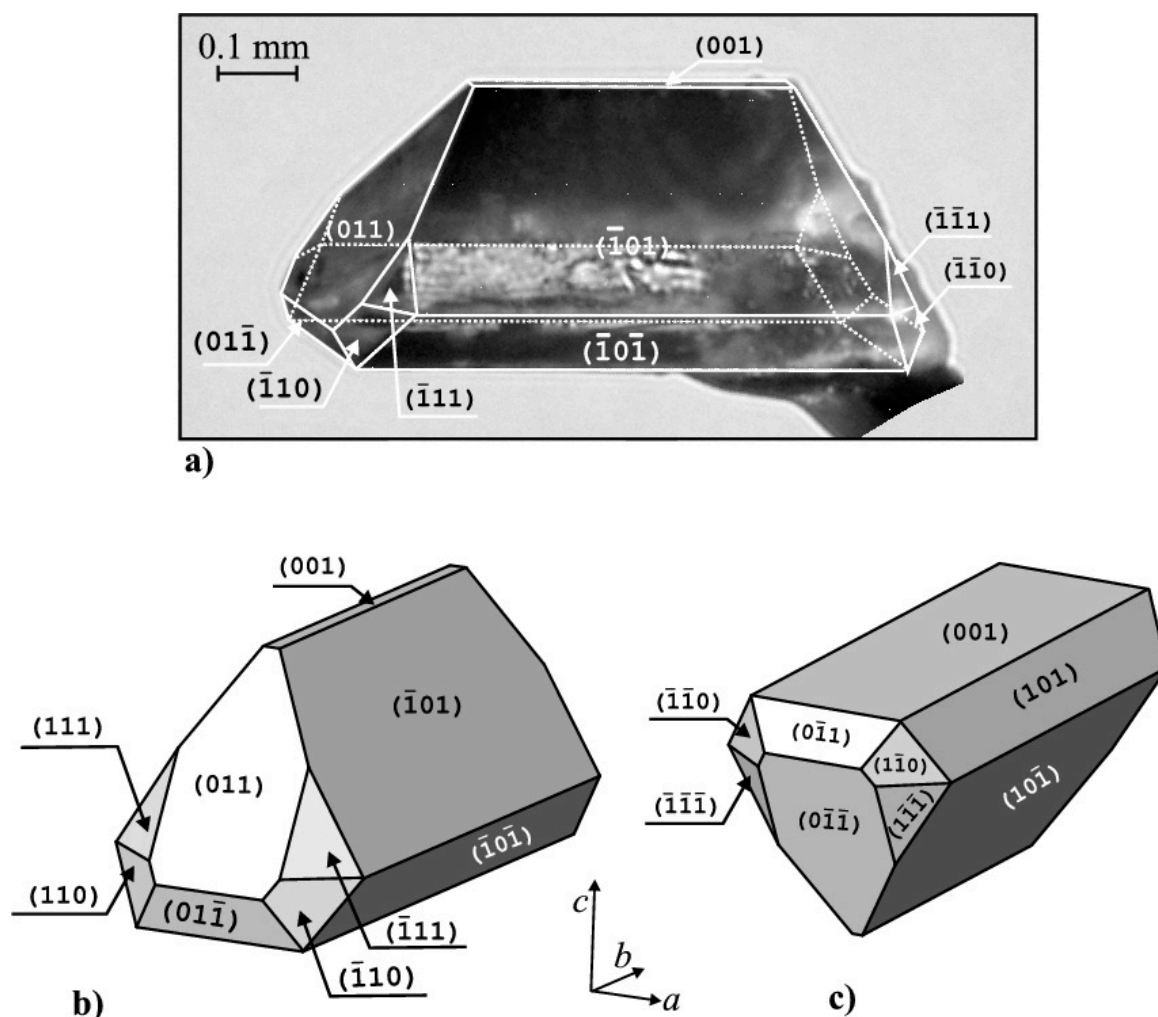


Figure 2. A view of struvite habit and morphology; (a) struvite grown in gel medium and (b) its schematic representation with faces indexed in accordance with the coordinate system assumed in this article; (c) faces indexed after transformation using the matrix given by Equation (2). Both polarities (b) and (c) are equivalent.

3.2. Crystal Structure

The crystal structure of struvite has been earlier reported by Whitaker and Jeffery [33], by Abbona, Calleri and Ivaldi [34] and by Tansman, Kindstedt and Hughes [35] on the basis of single crystal X-ray diffraction data as well as by Ferraris, Fuess and Joswig [36] on the basis of neutron diffraction data, all at room temperature. We decided to carry out measurements at temperature of 90 K, using hardware/software, enabling high data redundancy and accurate analytical numeric absorption corrections. As a result, we obtained a very high quality measurement with the residual factor R1 of 1.2% at 0.80 Å resolution. The x Flack parameter of $-0.01(2)$ was determined using 499 quotients [49].

As mentioned, XRD studies were carried out at 90 K. So far, low-temperature X-ray diffraction analysis for struvite in the context of phase transitions has not been carried out. Our research indicates a lack of polymorphism, resulting from the temperature lowering to 90 K, which has not been previously reported. Additionally, the study at 90 K allows reducing the standard uncertainty of the position of hydrogen atoms.

Struvite crystallizes in the orthorhombic polar noncentrosymmetric space group $Pmn2_1$ (No. 31). A view of the molecular structure with atom numbering scheme is depicted in Figure 3. The bond lengths and angles are in good agreement with the earlier results [33–36], but with appreciably

improved precision. Differences noted result from different temperatures of experiment or the use of another type of radiation (neutron vs. X-ray), in the case of the hydrogen atom positions.

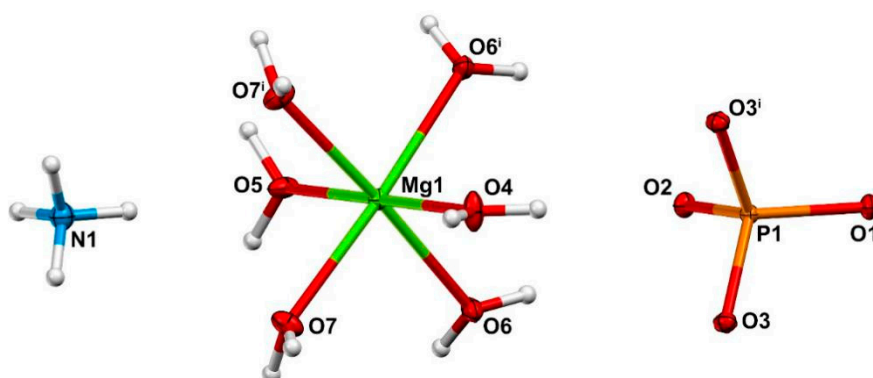


Figure 3. A view of the molecular structure of struvite with the atom numbering scheme. Symmetry code: (i) $-x,y,z$. Atomic displacement ellipsoids are drawn at 50% probability level. Hydrogen atoms are shown as small white spheres of arbitrary radius.

The crystal structure contains PO_4^- anions, hexaaqua $\text{Mg}(\text{H}_2\text{O})_6^{2+}$ cations and NH_4^+ cations connected within an extended three-dimensional hydrogen-bonded network of $\text{O-H}\cdots\text{O}$ and $\text{N-H}\cdots\text{O}$ (Figure 4). Geometric parameters including hydrogen-bonding have been previously described in [33]; here they are presented with higher accuracy and summarized in Tables 2 and 3.

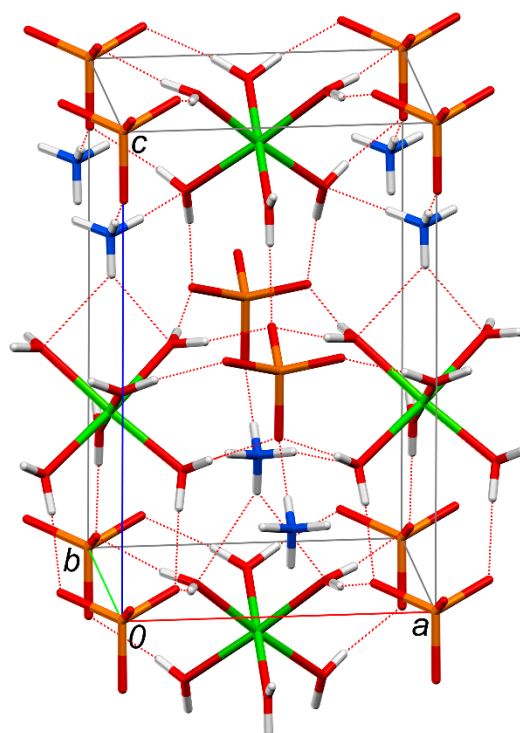


Figure 4. A fragment of molecular packing with the unit cell (with the coordinate system adopted in this study) showing the three-dimensional hydrogen-bond network marked with dotted lines.

Table 2. Bond lengths, selected bond valences and bond angles for struvite.

Bond Lengths (Å)		v.u.	Bond Angles (°)	
P1-O1	1.5508(15)		O1-P1-O2	109.55(7)
P1-O2	1.5468(13)		O1-P1-O3	109.55(4)
P1-O3	1.5441(9)		O2-P1-O3	108.74(4)
Mg1-O4	2.1071(14)	0.324	O3-P1-O3 ⁱ	110.69(5)
Mg1-O5	2.1090(14)	0.323	O4-Mg1-O5	179.82(6)
Mg1-O6	2.0751(11)	0.348	O4-Mg1-O6	91.17(4)
Mg1-O7	2.0511(11)	0.368	O4-Mg1-O7	90.44(4)
			O5-Mg1-O6	88.95(4)
			O5-Mg1-O7	89.44(4)
			O6-Mg1-O6 ⁱ	95.28(4)
			O6-Mg1-O7	87.66(4)
			O6-Mg1-O7 ⁱ	176.61(5)
			O7-Mg1-O7 ⁱ	89.34(5)

Symmetry code: ⁱ -x,y,z.**Table 3.** Hydrogen-bonding geometry in struvite.

D-H...A	D-H (Å)	H...A (Å)	D...A (Å)	D-H...A (°)	A Symmetry Code
O4-H1...O2	0.81(3)	1.87(3)	2.676(2)	179(3)	
O4-H2...O5	0.78(4)	2.23(4)	2.9986(19)	167(3)	x,y+1,z
O5-H3...O3	0.87(2)	1.79(2)	2.6588(11)	174(2)	1/2-x,1-y,1/2+z
O6-H4...O3	0.82(2)	1.81(2)	2.6336(13)	174(2)	x,y-1,z
O6-H5...O1	0.78(2)	1.92(2)	2.7017(13)	173(2)	1/2-x,1-y,1/2+z
O7-H6...O2	0.84(2)	1.80(2)	2.6264(12)	172(2)	1/2-x,1-y,1/2+z
O7-H7...O3	0.79(2)	1.88(2)	2.6544(12)	168(2)	1/2-x,3-y,1/2+z
N1-H8...O1	0.90(3)	1.90(3)	2.792(2)	179(3)	x,y-1,z+1
N1-H9...O7	0.89(4)	2.49(4)	3.1527(19)	131.3(19)	
N1-H10...O6	0.88(2)	2.137(19)	2.9726(17)	158.2(18)	1/2-x,1-y,1/2+z

The magnesium atom is surrounded by six oxygen atoms, creating a slightly elongated octahedron. The Cambridge Structural Database [50] reports 225 compounds with $\text{Mg}(\text{H}_2\text{O})_6^{2+}$ cations with the Mg-O bond length in the range of 2.012–2.151 Å with the mean value of 2.067 Å. It is worth noting that the longest of Mg-O bonds in struvite (2.1071 and 2.1090 Å) are on that upper limit. The relationship between bond length and bond valence, plays an important role in the study of the crystal structure in coordination chemistry.

A comparison of the chemical bond strengths of these bonds could be done using the related valence sum rule [51,52]. The Mg-O bond valences expressed in valence units (v.u.) were computed as $v_{ij} = \exp[(R_{ij} - d_{ij})/B]$ according to [53], where d_{ij} is bond length between atoms i - j , and R_{ij} is the bond-valence parameter, taken as $R_{\text{Mg-O}} = 1.608$ Å and $B = 0.443$ Å according to [54]. The oxidation state of magnesium resulting from the charge balance in the crystal should be equal +2. In fact, the calculated bond-valence sum (BVS) for Mg of 2.079 v.u. is slightly larger than expected, which is however in a good agreement, having the calculated the root-mean-square deviation value of 0.110 v.u. [54].

3.3. Thermoanalytical Study

Thermal decomposition of struvite is well known in literature (e.g., Refs. [37–40]). Although the shape of our TG curve is similar to that described in Refs. [37–40], the thermal stability and peaks on the DTA curve of struvite are significantly different from literature data. From our research, we can clearly see the endothermic peak and the appearance of a new exothermic effect. This exothermic peak has not been described in any previous studies on struvite. These differences indicate the desirability of our study. Thermal decomposition of struvite in air atmosphere is a multistage process. The stages of thermolysis overlap. Struvite is stable up to 85 °C. At first, struvite releases six molecules of water and an ammonium ion. On DTA curve there is an endothermic peak at 130 °C. Above 375 °C, MgHPO_4

is obtained as the final product of thermolysis (it is confirmed by XRD analysis of the sinter made by heating struvite to the temperature defined from the TG curve). This process connects with the exothermic effect on the DTA curve at 180 °C. Mass loss calculated is 50.98% and determined from the thermogravimetric curve is 51.00%, which confirms the formation of MgHPO_4 at the end of the thermal decomposition process. Figure 5 presents the TG-DTA-DTG curves of struvite. Pyrolysis of struvite at flowing air atmosphere with $40 \text{ mL}\cdot\text{min}^{-1}$ provides new information on its thermal decomposition.

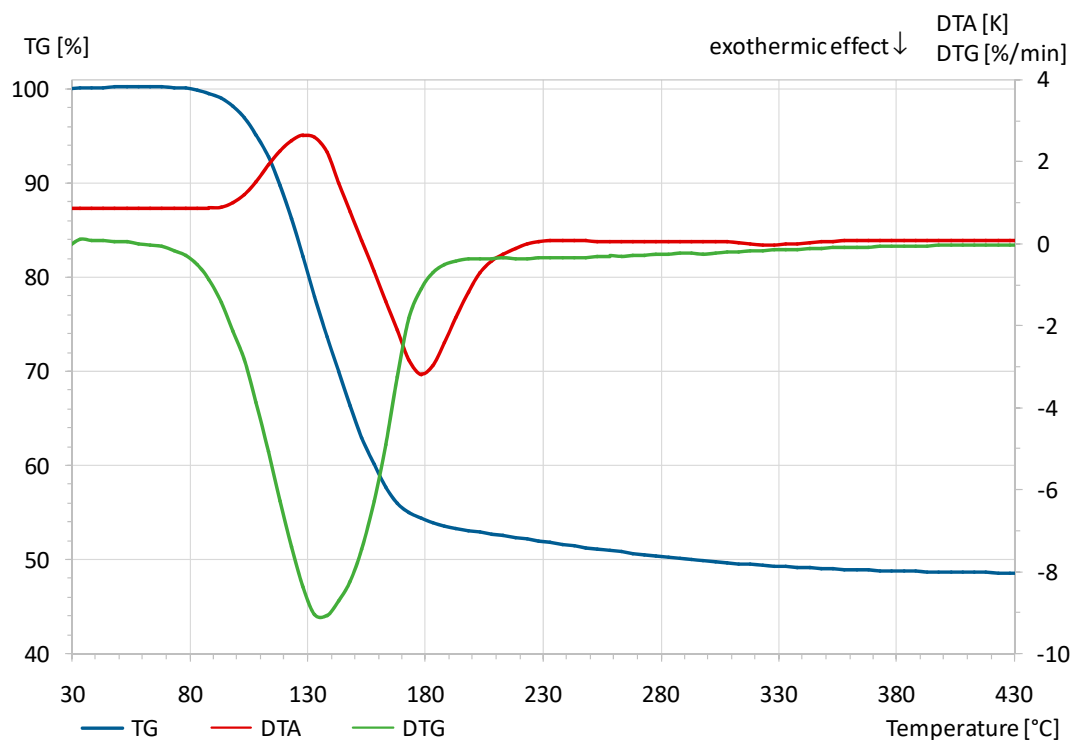


Figure 5. TG, DTA and DTG curves for struvite; the initial mass sample was 16.59 mg. The scale of the DTA and DTG curves is the same.

4. Conclusions

In this article we present struvite crystals grown from metasilicate gel using the single diffusion technique. The obtained crystals show a very rich morphology which consists of 18 faces. Most often, struvite crystals take prismatic habit. Grown crystals were examined and identified as pure struvite by single X-ray diffraction (XRD). The orthorhombic polar noncentrosymmetric space group $Pmn2_1$ was identified. The determined unit cell parameters are as follows $a = 6.9650(2) \text{ \AA}$, $b = 6.1165(2) \text{ \AA}$, $c = 11.2056(3) \text{ \AA}$. We obtained a very high quality results with the residual factor R1 of 1.2% at 0.80 Å resolution. XRD studies of struvite crystals were carried out at 90 K, while studies presented in the literature were carried out at room temperature. Our research shows that lowering the temperature to 90 K does not cause phase transitions. In other words, there are no polymorphic changes at low temperature. We also present thermoanalytical study of struvite using TG, DTG and DTA techniques. Our study differs from that described in Refs. [37–40]. In our case, we recorded a definitely different thermal stability (85 °C). Additionally, there was a shift of the endothermic peak compared to that described in Refs. [37–40]. A novelty in the thermal decomposition, has not been noted anywhere so far, is the appearance of an exothermic peak on the DTA curve (180 °C). Detection of endo- and exothermic peaks (not only an endothermic effect) during thermal decomposition of struvite gives new light on the pyrolysis of it.

Supplementary Materials: CCDC1885875 contains the supplementary crystallographic data for this paper. These data can be obtained free of charge from The Cambridge Crystallographic Data Centre via www.ccdc.cam.ac.uk/data_request/cif. The following are available online at <http://www.mdpi.com/2073-4352/9/2/89/s1>, Movie S1: The most typical prismatic habit of struvite crystals obtained by single diffusion gel growth technique (AVI).

Author Contributions: The contribution of J.P. covered the formulation of the problem of article; growing crystals from gel medium; analysis of their habit and morphology; managing a research project covering research being a problem of article; participation in writing the article. L.S. performed XRD measurements along with the interpretation of the results obtained and participated in writing the article. A.C. performed TG, DTA and DTG measurements and described their results.

Funding: This work was supported by the Ministry of Science and Higher Education (Poland), Grant No. I-3/501-17-3-1-728.

Conflicts of Interest: The authors declare no conflict of interest.

References

1. Henisch, H.K. *Crystal Growth in Gels*; The Pennsylvania State University Press: University Park, PA, USA; London, UK, 1970.
2. Lorber, B.; Sauter, C.; Theobald-Dietrich, A.; Moreno, A.; Schellenberger, P.; Robert, M.C.; Capelle, B.; Sanglier, S.; Potier, N.; Giege, R. Crystal growth of proteins, nucleic acids, and viruses in gels. *Prog. Biophys. Mol. Biol.* **2009**, *101*, 13–25. [[CrossRef](#)] [[PubMed](#)]
3. Otalora, F.; Gavira, J.A.; Ng, J.D.; Garcia-Ruiz, J.M. Counter diffusion methods applied to protein crystallization. *Prog. Biophys. Mol. Biol.* **2009**, *101*, 26–37. [[CrossRef](#)] [[PubMed](#)]
4. Bogorodskiy, A.; Frolov, F.; Mishin, A.; Round, E.; Polovinkin, V.; Cherezov, V.; Gordeliy, V.; Büldt, G.; Gensch, T.; Borshchevskiy, V. Nucleation and Growth of Membrane Protein Crystals in Meso—A Fluorescence Microscopy Study. *Cryst. Growth Des.* **2015**, *15*, 5656–5660. [[CrossRef](#)]
5. Cherezov, V.; Clogston, J.; Papiz, M.Z.; Caffrey, M. Room to Move: Crystallizing Membrane Proteins in Swollen Lipidic Mesophases. *J. Mol. Biol.* **2006**, *357*, 1605–1618. [[CrossRef](#)] [[PubMed](#)]
6. Foster, J.A.; Damodaran, K.K.; Maurin, A.; Day, G.M.; Thompson, H.P.G.; Cameron, G.J.; Bernal, J.C.; Steed, J.W. Pharmaceutical polymorph control in a drugmimetic supramolecular gel. *Chem. Sci.* **2017**, *8*, 78–84. [[CrossRef](#)] [[PubMed](#)]
7. Moreno, A.; Rosales-Hoz, M.J. Crystal growth of inorganic, organic, and biological macromolecules in gels. *Prog. Cryst. Growth Charact. Mater.* **2017**, *3*, 63–71. [[CrossRef](#)]
8. Chauhan, C.K.; Joshi, M.J. Growth inhibition of Struvite crystals in the presence of juice of Citrus medica Linn. *Urol. Res.* **2008**, *36*, 265–273. [[CrossRef](#)]
9. Manuel Bravo-Arredondo, J.; Moreno, A.; Mendoza, M.E. Crystal growth of cholesterol in hydrogels and its characterization. *J. Cryst. Growth* **2014**, *401*, 242–247. [[CrossRef](#)]
10. Ulex, G.L. On struvite, a new mineral. *Mem. Proc. Chem. Soc.* **1845**, *3*, 106–110. [[CrossRef](#)]
11. Lafuente, B.; Downs, R.T.; Yang, H.; Stone, N. The power of databases: The RRUFF project. In *Highlights in Mineralogical Crystallography*; Armbruster, T., Danisi, R.M., Eds.; W. De Gruyter: Berlin, Germany, 2015; pp. 1–30. Available online: <http://rruff.geo.arizona.edu/doclib/hom/struvite.pdf> (accessed on 20 January 2019).
12. Doyle, J.D.; Parsons, S.A. Struvite formation, control and recovery. *Water Res.* **2002**, *36*, 3925–3940. [[CrossRef](#)]
13. Brett, S.; Guy, J.; Morse, G.K.; Lester, J.N. *Phosphorous Removal and Recovery Technologies*; Selper Publications: London, UK, 1997.
14. Ye, Z.; Shen, Y.; Ye, X.; Zhang, Z.; Chen, S.; Shi, J. Phosphorus recovery from wastewater by struvite crystallization: Property of aggregates. *J. Environ. Sci.* **2014**, *26*, 991–1000. [[CrossRef](#)]
15. Booker, N.A.; Pristley, A.J.; Fraser, I.H. Struvite formation in wastewater treatment plants: Opportunities for nutrient recovery. *Environ. Technol.* **1999**, *20*, 777–782. [[CrossRef](#)]
16. Gaterell, M.R.; Gay, R.; Wilson, R.; Gochin, R.J.; Lester, J.N. An economic and environmental evaluation of the opportunities for substituting phosphorus recovered from wastewater treatment works in existing UK fertiliser markets. *Environ. Technol.* **2000**, *21*, 1067–1084. [[CrossRef](#)]
17. Jaffera, Y.; Clark, T.A.; Pearce, P.; Parsons, S.A. Potential phosphorous recovery by struvite formation. *Water Res.* **2002**, *36*, 1834–1842. [[CrossRef](#)]

18. Maqueda, C.; Perez Rodriguez, J.L.; Lebrato, J. Study of struvite precipitation in anaerobic digesters. *Water Res.* **1994**, *28*, 411–416. [CrossRef]
19. Ghos, G.; Mohan, K.; Sarkar, A. Struvite proves a good fertilizer. *CEEP Scope Newsl.* **2002**, *37*, 3–4.
20. Capdevielle, A.; Sýkorová, E.; Béline, F.; Daumer, M.L. Kinetics of struvite precipitation in synthetic biologically treated swine wastewaters. *Environ. Technol.* **2014**, *35*, 1250–1262. [CrossRef]
21. Weil, M. The struvite-type compounds $M[Mg(H_2O)_6](XO_4)$, where $M = Rb, Tl$ and $X = P, As$. *Cryst. Res. Technol.* **2008**, *43*, 1286–1291. [CrossRef]
22. Fang, C.; Zhang, T.; Jiang, R.; Ohtake, H. Phosphate enhance recovery from wastewater by mechanism analysis and optimization of struvite settle ability in fluidized bed reactor. *Sci. Rep.* **2016**, *6*, 32215. [CrossRef]
23. Strickland, J. Perspectives for phosphorous recovery offered by enhanced biological removal. *Environ. Technol.* **1999**, *20*, 721–725. [CrossRef]
24. Abbona, F. Crystallization of calcium and magnesium phosphates from solution of low concentration. *J. Cryst. Growth* **1997**, *104*, 661–671. [CrossRef]
25. Bridger, G. Fertilizer value of struvite. *CEEP Scope Newsl.* **2001**, *43*, 3–4.
26. Bichler, K.H.; Eipper, E.; Naber, K.; Braun, V.; Zimmermann, R.; Lahme, S. Urinary infection stones. *Int. J. Antimicrob. Agents* **2002**, *19*, 488–498. [CrossRef]
27. Gleeson, M.J.; Griffith, D.P. Struvite calculi. *Br. J. Urol.* **1993**, *71*, 503–511. [CrossRef] [PubMed]
28. Griffith, D.P.; Musher, D.M.; Itin, C. Urease. The primary cause of infection-induced urinary stones. *Investig. Urol.* **1976**, *13*, 346–350.
29. McLean, R.J.C.; Nickel, J.C.; Cheng, K.J.; Costerton, J.W. The ecology and pathogenicity of urease-producing bacteria in the urinary tract. *CRC Crit. Rev. Microbiol.* **1988**, *16*, 37–79. [CrossRef] [PubMed]
30. Leusmann, D.B.; Sabinski, F. Potential contribution of optional urease-positive bacteria to idiopathic urinary calcium stone formation. *Urol. Res.* **1996**, *24*, 73–78. [CrossRef] [PubMed]
31. Chauhan, C.K.; Joshi, M.J. In vitro crystallization, characterization and growth inhibition study of urinary type struvite crystals. *J. Cryst. Growth* **2013**, *362*, 330–337. [CrossRef]
32. Website of e-Medicine (Medscape): Struvite and Staghorn Calculi. Available online: <http://emedicine.medscape.com/article/439127> (accessed on 18 December 2018).
33. Whitaker, A.; Jeffery, J.W. The Crystal Structure of Struvite, $MgNH_4PO_4 \cdot 6H_2O$. *Acta Crystallogr. Sect. B* **1970**, *26*, 1429–1440. [CrossRef]
34. Abbona, F.; Calleri, M.; Ivaldi, G. Synthetic Struvite, $MgNH_4PO_4 \cdot 6H_2O$: Correct Polarity and Surface Features of Some Complementary Forms. *Acta Crystallogr. Sect. B* **1984**, *40*, 223–227. [CrossRef]
35. Tansman, G.F.; Kindstedt, P.S.; Hughes, J.M. Minerals in Food: Crystal Structures of Ikaite and Struvite from Bacterial Smears on Washed-Rind Cheese. *Can. Mineral.* **2017**, *55*, 89–100. [CrossRef]
36. Ferraris, G.; Fuess, H.; Joswig, W. Neutron Diffraction Study of $MgNH_4PO_4 \cdot 6H_2O$ (Struvite) and Survey of Water Molecules Donating Short Hydrogen Bonds. *Acta Crystallogr. Sect. B* **1986**, *42*, 253–258. [CrossRef]
37. Ramlogan, M.V.; Rouff, A.A. An investigation of the thermal behavior of magnesium ammonium phosphate hexahydrate. *J. Therm. Anal. Calorim.* **2016**, *123*, 145–152. [CrossRef]
38. Chen, Y.; Tang, J.; Li, W.; Zhong, Z.; Yin, J. Thermal decomposition of magnesium ammonium phosphate and adsorption properties of its pyrolysis products toward ammonia nitrogen. *Trans. Nonferrous Met. Soc. China* **2015**, *25*, 497–503. [CrossRef]
39. Yu, R.; Ren, H.; Wang, Y.; Ding, L.; Geng, J.; Xu, K.; Zhang, Y. A kinetic study of struvite precipitation recycling technology with $NaOH/Mg(OH)_2$ addition. *Bioresour. Technol.* **2013**, *143*, 519–524. [CrossRef] [PubMed]
40. Ma, N.; Rouff, A.A.; Phillips, B.L. A ^{31}P NMR and TG/DSC-FTIR Investigation of the Influence of Initial pH on Phosphorus Recovery as Struvite. *ACS Sustain. Chem. Eng.* **2014**, *4*, 816–822. [CrossRef]
41. Rigaku, O.D. *CrysAlis PRO*; Rigaku Oxford Diffraction Ltd.: Yarnton, UK, 2016.
42. Sheldrick, G.M. SHELXT—Integrated space-group and crystal-structure determination. *Acta Crystallogr. Sect. A* **2015**, *71*, 3–8. [CrossRef]
43. Sheldrick, G.M. Crystal structure refinement with SHELXL. *Acta Crystallogr. Sect. C* **2015**, *71*, 3–8. [CrossRef]
44. Wierzbicki, A.; Sallis, J.D.; Stevens, E.D.; Smith, M.; Sikes, C.S. Crystal Growth and Molecular Modeling Studies of Inhibition of Struvite by Phosphocitrate. *Calcif. Tissue Int.* **1997**, *61*, 216–222. [CrossRef]
45. Prywer, J.; Torzewska, A. Bacterially Induced Struvite Growth from Synthetic Urine: Experimental and Theoretical Characterization of Crystal Morphology. *Cryst. Growth Des.* **2009**, *9*, 3538–3543. [CrossRef]

46. Sadowski, R.R.; Prywer, J.; Torzewska, A. Morphology of struvite crystals as an evidence of bacteria mediated growth. *Cryst. Res. Technol.* **2014**, *49*, 478–489. [[CrossRef](#)]
47. Dominick, M.A.; White, M.R.; Sanderson, T.P.; Van Vleet, T.; Cohen, S.M.; Arnold, L.E.; Cano, M.; Tannehill-Gregg, S.; Moehlenkamp, J.D.; Waites, C.R.; et al. Urothelial carcinogenesis in the urinary bladder of male rats treated with muraglitazar, a PPAR alpha/gamma agonist: Evidence for urolithiasis as the inciting event in the mode of action. *Toxicol. Pathol.* **2006**, *34*, 903–920. [[CrossRef](#)] [[PubMed](#)]
48. Abbona, F.; Boistelle, R. Growth morphology and crystal habit of struvite crystals ($\text{MgNH}_4\text{PO}_4 \cdot 6 \text{H}_2\text{O}$). *J. Cryst. Growth* **1979**, *46*, 339–354. [[CrossRef](#)]
49. Parsons, S.; Flack, H.D.; Wagner, T. Use of intensity quotients and differences in absolute structure refinement. *Acta Crystallogr. Sect. B* **2013**, *69*, 249–259. [[CrossRef](#)] [[PubMed](#)]
50. Groom, C.R.; Bruno, I.J.; Lightfoot, M.P.; Ward, S.C. The Cambridge Structural Database. *Acta Crystallogr. Sect. B* **2016**, *72*, 171–179. [[CrossRef](#)] [[PubMed](#)]
51. Brown, I.D. Bond-Length-Bond-Valence Relationships in Inorganic Solids. In *Structure Correlation, Part III*; Burgi, H.-B., Dunitz, J.D., Eds.; VCH Publishers: Weinheim, Germany; New York, NY, USA, 1994; pp. 405–429.
52. Brown, I.D. Chemical and steric constraints in inorganic solids. *Acta Crystallogr. Sect. B* **1992**, *48*, 553–572. [[CrossRef](#)]
53. Brown, I.D. Influence of Chemical and Spatial Constraints on the Structures of Inorganic Compounds. *Acta Crystallogr. Sect. B* **1997**, *53*, 381–393. [[CrossRef](#)]
54. Gagnéa, O.C.; Hawthorne, F.C. Bond-length distributions for ions bonded to oxygen: Metalloids and post-transition metals. *Acta Crystallogr. Sect. B* **2015**, *71*, 562–578. [[CrossRef](#)]



© 2019 by the authors. Licensee MDPI, Basel, Switzerland. This article is an open access article distributed under the terms and conditions of the Creative Commons Attribution (CC BY) license (<http://creativecommons.org/licenses/by/4.0/>).